

Flow regimes and wall shear rates determination within a scraped surface heat exchanger

Eric Dumont^{a,b}, Francine Fayolle^{a,*}, Jack Legrand^b

^a *Ecole Nationale Supérieure d'Ingénieurs des Techniques Agricoles et Alimentaires, Département Génie des Procédés Alimentaires, Rue de la Géraudière, BP 82225, 44322 Nantes Cedex 3, France*

^b *Laboratoire de Génie des Procédés, UPRES EA 1152, Université de Nantes, CRTT, BP 406, 44602 Saint Nazaire Cedex, France*

Received 30 July 1999; accepted 6 March 2000

Abstract

An experimental investigation of a scraped surface heat exchanger (SSHE) was undertaken using visual observations and the electrochemical technique in order to, firstly, study the transition between laminar and vortex flows and, secondly, evaluate the wall shear rates. Visual observations and the electrochemical technique had undergone preliminary testing in a SSHE without blades, a well-known reference annulus. Then, visual observations and wall shear rates was compared in both geometries. It was established that flow patterns in a SSHE are noticeably different from those observed in an annular space in the same conditions. In a SSHE, the formation of the vortices is thwarted by the rotation of the blades (and by the clips of the blades) and the transition between laminar and vortex flows occurs at $Ta_{gc} \approx 80$ ($Ta_{gc} \approx 45$ in the annular space without blades). Local measurements of the shear rate at the tube wall of the SSHE showed that it is fully controlled by the rotation of the blades. Vortices have a negligible influence in comparison with that of blade scrapings. Wall shear rates due to blade scraping can reach up to $40\,000\text{ s}^{-1}$. Under these conditions, the lowest value of the clearance between the edge of the blades and the stator is about $50 \times 10^{-6}\text{ m}$. © 2000 Elsevier Science Ltd. All rights reserved.

Keywords: Scraped surface heat exchanger; Flow patterns; Vortex flow; Microelectrode; Visual analysis; Wall shear rates

1. Introduction

Scraped surface heat exchangers (SSHE), mainly used in the food industry, allow highly viscous fluids with complex rheology (cream cheese, fruit concentrate, ice cream, among others) to be processed. The first advantage of these exchangers lies in the rotation of a shaft equipped with blades which periodically scrape the exchange surface in order to prevent crust formation and to promote heat transfer (Fig. 1). The second one lies in the geometry of the inlet and outlet bowls. In this type of exchanger, the flow is the result of the superposition of a Poiseuille flow in an annular space and a Couette flow, on which perturbations created by the blades are added. This flow pattern is particularly complex and has only been superficially studied directly (Trommelen & Beek, 1971a; Naimi, 1989; Burmester, Winch & Russel, 1996). Most of the works on the subject tend to model the

geometry of the SSHE as an annular space without blades, where the hydrodynamics are well known (Härröd, 1986; Abichandani, Sarma & Heldman, 1987). Depending on the rotational speed of the rotor, two different flow regimes can be shown: laminar or vortex flow. Without blades, the change between these two regimes is due to the appearance of vortices at a critical value of generalised Taylor number (Ta_{gc}) varying with the radius ratio (R_r/R_s ; Esser & Grossmann, 1996), increasing with the axial flow rate (Re_{axg} ; DiPrima, 1960) and depending on the rheological properties of the product used (Wronski & Jastrzebski, 1990). From the vast literature on non-Newtonian annular flow (Giordano, Giordano, Prazeres & Cooney, 1998), it can be expected that plug flow conditions may occur in a SSHE when the flow is vortical but close to the laminar flow regime (Härröd, 1990a). Härröd (1990b) experimentally verified that the most favourable flow pattern in a SSHE occurs at these conditions. Härröd (1990a) also indicates that the most favourable flow pattern is obtained by a slight increase of the rotational speed. Thus, it is important to distinguish between laminar and vortex flow

* Corresponding author. Tel.: +33-2-51-78-54-80; fax: +33-2-51-78-54-67.

E-mail address: fayolle@enitaa-nantes.fr (F. Fayolle).

Nomenclature			
C_0	bulk concentration (mol m ⁻³)	S_c	“corrected” wall shear rate (s ⁻¹)
D	diffusion coefficient (m ² s ⁻¹)	S_m	wall shear rate at the inflow boundary in an annulus (s ⁻¹)
d	diameter of the microelectrode (m)	S_M	wall shear rate at the outflow boundary in an annulus (s ⁻¹)
d_h	hydraulic diameter (m); $d_h = (d_s - d_r)$	S_{max}	maximal value of the shear rate at the tube wall of the SSHE (s ⁻¹)
d_r	rotor diameter (m)	S_{min}	minimum value of the shear rate at the tube wall of the SSHE (s ⁻¹)
d_s	stator diameter (m)	S_p	wall shear rate (s ⁻¹)
e	gap (m)	t_0	characteristic time of the microelectrode (s)
F	Faraday constant (A s mol ⁻¹)	T	temperature (°C)
I	limiting diffusion current (A)	$Ta = \sqrt{\frac{R_s - R_r}{R_r} \frac{\rho d_h}{2} \frac{(\Omega R_r)}{\mu}}$	Taylor number (dimensionless)
K	consistency coefficient of the product (Ostwald law; Pa s ⁿ)	$Ta_g = \sqrt{\frac{R_s - R_r}{R_r} \frac{\rho d_h^n}{2^n} \frac{(\Omega R_r)^{2-n}}{K}}$	generalised Taylor number (dimensionless)
l	characteristic dimension of the probe along the direction of the velocity fluctuations (m)	Ta_c, Ta_{gc}	critical values of Taylor numbers (dimensionless)
L	stator length (m)	U_d	mean axial velocity in the annular space (m s ⁻¹)
n	flow behavior index of the product (Ostwald law; dimensionless)	z	number of electrons (dimensionless)
N	rotational speed (rpm ⁻¹)	$\dot{\gamma}$	shear rate (s ⁻¹)
n_L	number of blades (dimensionless)	δ	clearance between the edge of the blade and stator (m)
Q	flow rate (m ³ s ⁻¹)	μ	dynamic viscosity for Newtonian fluid (Pa s)
$Re_{ax} = \frac{\rho U_d d_h}{\mu}$	axial Reynolds number (dimensionless)	ρ	density (kg m ⁻³)
$Re_{axg} = \frac{\rho U_d^{2-n} d_h^n}{K}$	generalised axial Reynolds number (dimensionless)	Ω	rotating speed of the rotor (rad s ⁻¹)
R_r	rotor radius (m)		
R_s	stator radius (m)		
\bar{S}	average wall shear rate in an annulus (s ⁻¹)		
S	local wall shear rate (s ⁻¹)		

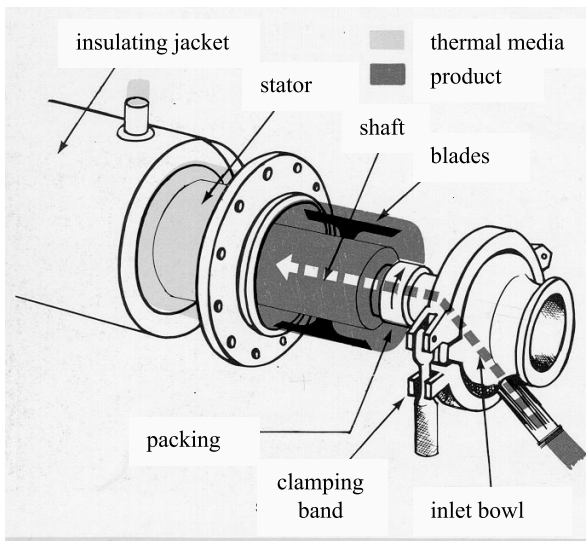


Fig. 1. Principal design of SSHE (by courtesy of Duprat company).

in industrial applications in order to promote efficient mixing and to optimise the rotational speed. Unfortunately, the mechanical fragility of treated products sometimes induces working constraints which do not permit a sufficient rotational speed to allow vortex flow and correct mixing. In this case, some of the products treated in the exchangers show high temperature heterogeneities. Industrially, heterogeneities can reach up to 30°C (Härröd, 1990c). For this author, the weak heat transformation of the product is due to both flow regime and shape of the shaft and blades. Temperature mea-

surements in both inlet and outlet bowls, which characterise radial and axial mixing in the exchanger, seems the best way to emphasise the transition between the different flow patterns in an industrial SSHE (Miyachi & Vermulen, 1963; Härröd, 1990a). A previous paper (Dumont, Della Valle, Fayolle & Legrand, 2000a) deals with the thermal evolution of model fluids, Newtonian and non-Newtonian, in heating or cooling conditions within an industrial SSHE, and allows us to link the phenomena of appearance and disappearance of temperature heterogeneities with the changes in the flow pattern within the exchanger. Based on literature data dedicated to SSHEs as well as to annular spaces without blades (Dumont et al., 2000a), we show that thermally homogeneous products can be obtained when Taylor vortices appear in the exchanger. Studies done on the exchanger with and without blades show that the thermal behaviour is basically the same for both geometries but with a difference in critical generalised Taylor numbers value for vortex appearance. The presence of the blades should promote the appearance of instabilities at lower values of the generalised Taylor number ($Ta_{gc} = 10$ with blades; $Ta_{gc} = 39$ without blades; industrial SSHE).

The aims of this paper are, firstly, to observe by visualisation the transition between laminar and vortex flows in order to verify the hypothesis that presence of blades should promote the appearance of instabilities, and secondly, to determine by means of an electrochemical technique the wall shear rates generated by the rotation of the blades. A preliminary study is carried out

in the SSHE without blades (i.e., an annular space which represents a well-known reference geometry) in order to validate results given by visual observations and the electrochemical method.

2. Materials and method

2.1. Scaled-down model of SSHE

The work was carried out on a scaled-down model of the Duprat TR 13×60 industrial exchanger. All dimensions are given in Table 1. The scaled-down model was used to fulfil visual analyses in order to understand the part played by the rotational speed and the geometrical elements of the exchanger (bowls, shaft and blades) in the transition between laminar and vortex flows. But, this scaled-down model had also to allow extrapolation of the results obtained for the model up to the industrial scale. Thus, the scaled-down was built in order to present the same thermal behaviour as the industrial SSHE (with variations of the temperature heterogeneities; Dumont, Fayolle & Legrand, 1999). The design principle used was the retain of the Ta_g order of magnitude found in the industrial exchanger ($0 < Ta_g < 100$) when keeping rotational speed at industrial values ($0 < N < 10 \text{ s}^{-1}$). The shaft and stator diameters were chosen to be half the ones of the industrial apparatus (which keeps a constant d_r/d_s ratio). The exchanger volume was calculated taking into account the axial flowing velocity which was chosen, for a given flowrate, in order to keep the same residence time as in the industrial apparatus. The stator length determined in this way (Table 1) represented a compromise at half scale of two different lengths commonly used in the food industry ($L/d_s \approx 2.3\text{--}7.7$). Scaled-down model of the SSHE, shown in Fig. 2, allowed the handling of thermal studies (stator and insulating jacket in stainless steel), visualisations and wall shear rates studies (stator of transparent altuglass).

Visualisations and wall shear rates studies were carried out under isothermal conditions ($T = 25^\circ\text{C}$). The

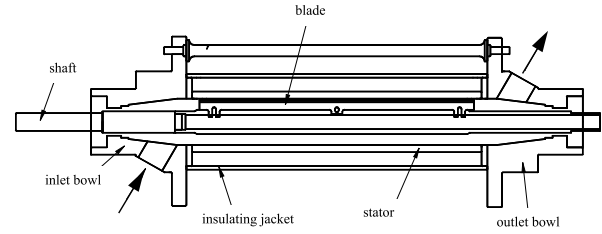


Fig. 2. Scaled-down model of the SSHE.

pilot plant included: an inlet tank, a pump, the scaled-down model of the exchanger, a Promag (Endress Hauser) electromagnetic flowmeter and an experimental apparatus for electrochemical technique.

2.2. Electrochemical method

Wall shear rates were determined with an electrical method. The principle consists in measuring the electrical current I delivered by a platinum microelectrode which results from a very fast redox reaction: $\text{Fe}(\text{CN}_6)^{3-} + e^- \leftrightarrow \text{Fe}(\text{CN}_6)^{4-}$ with a large excess of supporting electrolyte K_2SO_4 so as to eliminate the migration current due to the electric field. A voltage difference ΔV is set between the probe (the working electrode) and a large counter electrode (the shaft). If ΔV is large enough on the microelectrode, the concentration of the reacting ion tends to zero and the current attains a limit value I . This limiting current is fully controlled by diffusion only. If the length of the microelectrode is very small in the flow direction, the concentration boundary layer on the electrode is thin; thus, the flow velocity linearly varies throughout the thickness of this boundary layer. If the flow fluctuations are slow enough, the quasi-steady relation can be applied to relate the wall shear rate, S , to the limiting diffusion current, I (Reiss & Hanratty, 1963)

$$S = \left(\frac{1.477}{zF} \right) \frac{I^3}{D^2 C_0^3 d^5}, \quad (1)$$

where z is the number of electrons involved in the redox reaction, F the Faraday constant, d the diameter of the circular microelectrode, C_0 the bulk concentration of the active ions and D is the diffusion coefficient of these ions in solution. The limiting diffusion current was measured on 12 0.4 mm-diameter circular microelectrodes embedded axially on the outer cylinder surface (Fig. 3).

2.3. Characteristics of the electrolytes

Three polymeric solutions were used to carry out the experiments: one Newtonian fluid and two shear-thinning fluids. The viscosity measurements were performed at 25°C with a Couette rheometer TA Instrument AR 1000 with imposed torque. The fluids were chosen with

Table 1
Geometrical characteristics of industrial SSHE and its scaled-down model

	Industrial SSHE (1)	Scaled-down model (2)	Ratio (1)/(2)
Stator diameter (d_s)	0.13 m	0.065 m	2
Stator length (L)	0.60 m	0.38 m	1.58
Ratio (L/d_s)	4.61	5.85	0.79
Rotor diameter (d_r)	0.080 m	0.040 m	2
Ratio (d_r/d_s)	0.615	0.615	1
Gap $e = (d_s - d_r)/2$	0.025 m	0.0125 m	2
Exchange surface	0.245 (m^2)	7.76×10^{-2} (m^2)	3.16

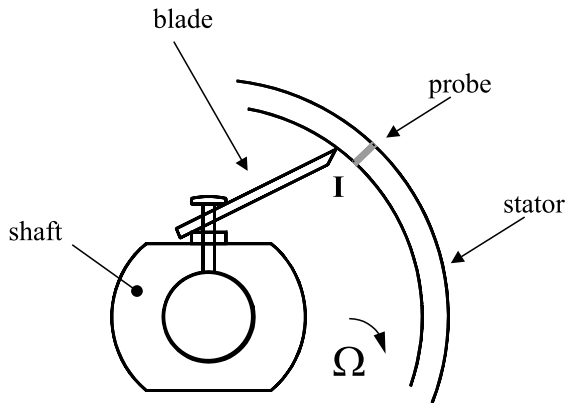


Fig. 3. Schematic representation of a microelectrode embedded on outer cylinder.

particular care. Indeed, it was difficult to make highly viscous solutions complying with the restraints of the electrochemical method (dissolution of salts in sufficient quantities, chemically inert fluid and model fluid not too far away from a food product).

Emkarox HV 45, from ICI, is a mixture of polypropylene glycol and polyethylene glycol. The dynamic viscosity of the pure products is equal to 3.7 Pa s at 25°C. The electrolyte was composed of a mixture of potassium ferricyanide, potassium ferrocyanide and potassium sulphate as supporting electrolyte. The viscosities of the different aqueous solutions are given in Table 2. We also studied a low-viscosity solution, polyethylene glycol (PEG) 35000. Visual observations were carried out on these solutions mixed with Kalliroscope and their Newtonian behaviour was checked.

Aqueous solutions of carboxymethylcellulose (CMC from Sigma) have a pseudoplastic behaviour. The non-Newtonian characteristics depend on the CMC concentration. CMC powder was progressively added in agitated cold water. After dissolution of carboxymethylcellulose sodium salt, potassium sulphate and potassium ferri- and ferrocyanide were added to the electrolyte. The rheological behaviour was modelled by two different power-laws according to the shear rate domains: 5–80 and 50–1230 s⁻¹. The physical properties of CMC electrolyte are given in Table 3.

Table 2
Physical properties of Emkarox HV45 solutions at 25°C

Solution	Water (w/w, %)	K ₃ [Fe(CN) ₆] (mol m ⁻³)	K ₄ [Fe(CN) ₆] (mol m ⁻³)	K ₂ SO ₄ (mol m ⁻³)	ρ (kg m ⁻³)	μ (Pa s)	D × 10 ¹⁰ (m ² s ⁻¹)
HV45-80	20	5.327	5.327	106.5	1080	1.18	0.51
HV45-75	25	5.304	5.304	127.3	1079	0.84	0.70
HV45-70	30	5.283	5.283	158.5	1077	0.60	0.82
HV45-65	35	5.262	5.262	210.5	1073	0.43	1.00
HV45-60	40	5.241	5.241	209.6	1071	0.32	1.15
HV45-55	45	5.220	5.220	229.7	1070	0.23	1.35
PEG	–	5.000	5.000	250.0	1058	0.04	3.50

The preparation of guar gum solutions was similar to that of the CMC solutions, except that the guar gum dissolution was at 40°C. Two power-law equations were proposed to model the non-Newtonian behaviour of guar gum solutions: one for shear rates from 2 to 20 s⁻¹ and the second for 10 to 1230 s⁻¹. Rheological data is summarised in Table 3. Special attention was given for the determination of the diffusion coefficients of ferricyanide ions in these polymeric solutions (Legrand, Dumont, Comiti & Fayolle, 2000).

2.4. Operating conditions

Each experiment was done as follows: flow rate ($Q = 35 \text{ l h}^{-1}$), rotational speed of the rotor (N varied from 30 to 600 rpm) and product temperature ($T = 25^\circ\text{C}$) before the inlet were adjusted to the desired values. For each rotational speed, the limiting diffusion currents from the microelectrodes were numerically recorded over 90 s (laminar flow) or over 150 s (vortex flow). The generalised axial Reynolds number (Re_{axg}) and generalised Taylor number (Ta_g) were used to characterise the flow pattern. Visual observations were carried out on Newtonian solutions mixed with Kalliroscope AQ 1000 from Kalliroscope Corporation. Kalliroscope fluid is a suspension of microscopic crystalline platelets which are oriented so as to align their larger dimensions parallel to the streamlines. In the presence of incident light, areas of varying orientation reflect differing light intensities and their variation and movement produce striking visual images of the streamlines.

3. Results and discussion

3.1. Flow patterns

3.1.1. Without blades

The flow stability investigations consist of determining the dependence of the limiting current value I on the angular velocity Ω of the shaft. At the beginning, the value of I is constant with the time (Fig. 4), which is interpreted as flow without vortices. When a certain

Table 3
Physical properties of CMC and guar solutions at 25°C

Solution weight (%)	ρ (kg m ⁻³)	K ₃ [Fe(CN) ₆] (mol m ⁻³)	K ₄ [Fe(CN) ₆] (mol m ⁻³)	K ₂ SO ₄ (mol m ⁻³)	$D \times 10^{10}$ (m ² s ⁻¹)	Shear rate domain $\dot{\gamma}$ (s ⁻¹)			
						5–80		50–1234	
						n	K (Pa s ^{<i>n</i>})	n	K (Pa s ^{<i>n</i>})
CMC 0.5	1046	5.0	5.0	300	7.50	0.85	0.11	0.73	0.16
CMC 0.7	1071	5.0	5.0	500	7.50	0.78	0.36	0.65	0.63
CMC 0.9	1047	5.0	5.0	300	7.50	0.70	1.05	0.55	1.98
CMC 1.0	1047	4.0	4.0	300	7.50	0.66	1.64	0.51	3.02
CMC 1.1	1048	4.0	4.0	300	7.50	0.62	2.49	0.48	4.44
						Shear rate domain $\dot{\gamma}$ (s ⁻¹)			
						2–20		10–1234	
Guar 0.7	1046	3.0	3.0	300	6.90	0.65	0.78	0.47	1.31
Guar 0.8	1046	4.0	4.0	300	6.90	0.63	1.21	0.44	2.04
Guar 1.0	1043	5.0	5.0	300	6.90	0.51	3.29	0.36	4.86
Guar 1.2	1047	5.0	5.0	300	6.90	0.44	6.40	0.32	8.91

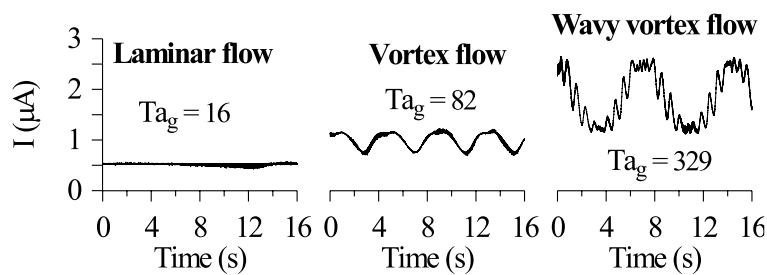


Fig. 4. Examples of record of limiting diffusion current with respect to time in an annulus without blades for a Newtonian solution ($Q = 35 \text{ l h}^{-1}$; $Re_{axg} = 3.1$).

value of rotational speed is reached, a sudden transformation in I appears. The limiting current value presents a periodic form (Fig. 4) attributed to the onset of the instability ($Ta_g \approx 45$). The maximum value of I corresponds to the separation line of two vortices of the same pair at the surface of the stator (maximum value of wall shear rate S_M ; Fig. 5) while the minimum value corresponds to the junction between two pairs of vortices (in that case, the wall shear rate is minimum, S_m , at the surface of the stator; Fig. 5). This interpretation is confirmed by visual experiments carried out with HV45 Emkarox solutions. It is found that the change in the limiting current evolution corresponds well to the appearance of Taylor vortices (Fig. 6). In this flow, toroidal vortices encircle the inner cylinder and move through the annulus without being disturbed by the axial flow. The results obtained for very small values of axial flow velocity U_d can be applied in stability analysis of Couette flow ($U_d = 0$). When Ta_g exceeds about 240, the limiting current value shows a double periodic variation (Fig. 4) which indicates the generation of a new vortex flow characterised by wavy oscillations.

These oscillations are generated by a disturbance formed inside the inlet bowl near the inner cylinder. Figs. 6 and 7 allow understanding the phenomenon. Without axial flow (Fig. 6), Taylor vortices are always perfectly formed in the annulus with increase of Ta_g . But, when

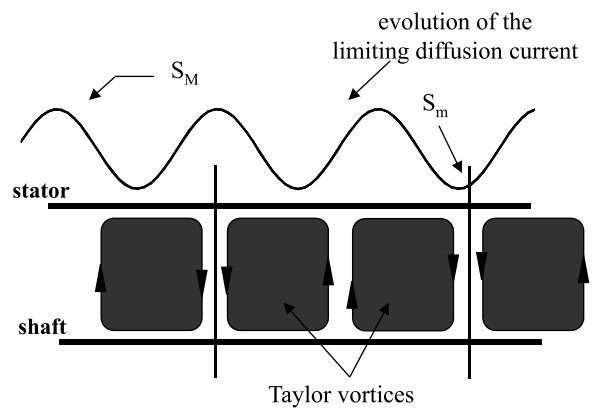


Fig. 5. Schematic representation of Taylor vortices in an annulus without blades.

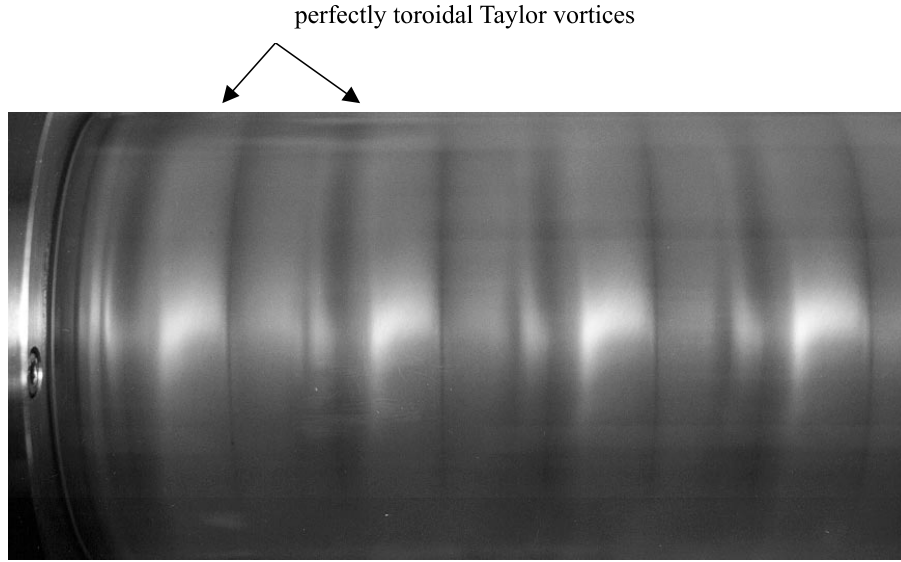


Fig. 6. View of Taylor vortices at the inlet of the annulus without axial flow for a Newtonian solution (no blades; $Ta_g = 180$; $N = 10$ rps; $Q = 0.1 \text{ h}^{-1}$; $Re_{axg} = 0$). Flow pattern without perturbation.

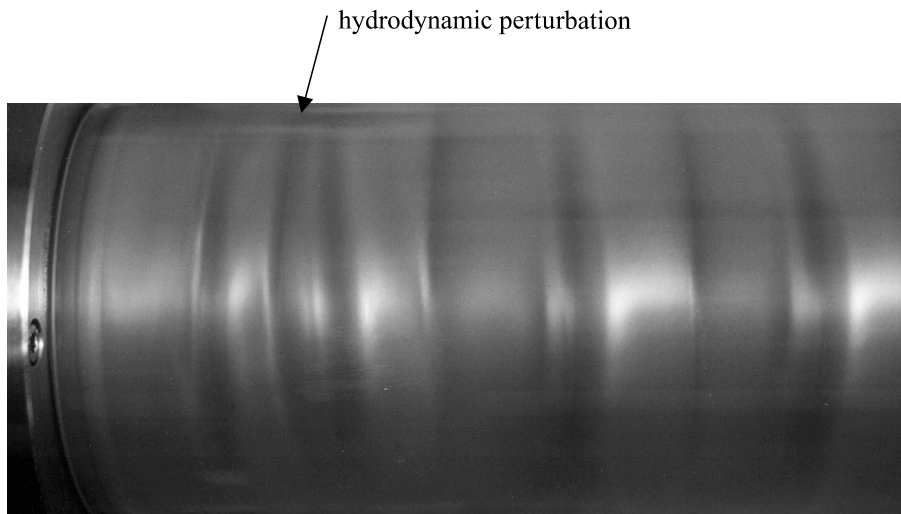


Fig. 7. Hydrodynamic perturbation located at the inlet of the annulus with axial flow and for a Newtonian solution (no blades; $Ta_g = 180$; $N = 10$ rps; $Q = 35 \text{ l h}^{-1}$; $Re_{axg} = 1.7$).

axial flow is added to rotational flow, the change of shaft diameter at the inlet of the annulus (Fig. 1) gives a hydrodynamic perturbation (Fig. 7). When Ta_g is gradually raised, visual observations show that the disturbance concerns only in the first five centimetres of the annulus until a critical value ($Ta_g \approx 240$) as the disturbance travels axially towards the outlet and creates a doubly periodic flow.

3.1.2. With 2 blades

In the scaled-down model of the SSHE, with blades mounted on the inner rotating cylinder, with axial flow and no heat transfer, visual investigations show that

the flow stays laminar over a large range of Ta_g (up to 80). For more important values of Ta_g , flow structure presents a vortex pattern (Fig. 8) but vortices are thwarted by the rotation of the blades and three symmetrical zones appear at the ends of the equipment (Fig. 9):

- zone a (first clip of the blades on the shaft): there are no vortices in the flow pattern,
- zone b: perturbed zone where small vortices are growing to give birth to Taylor cells. A part of the created vortices flows in the direction of zone a where it disappears; the other part progresses axially in the scaled-down under the action of the flowrate,

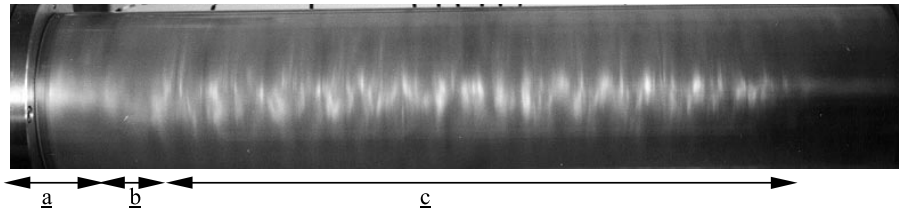


Fig. 8. View of vortex flow in SSHE for a Newtonian solution (2 blades; $Ta_g = 113$; $N = 6$ rps; $Q = 35 \text{ l h}^{-1}$; $Re_{axg} = 1.9$).

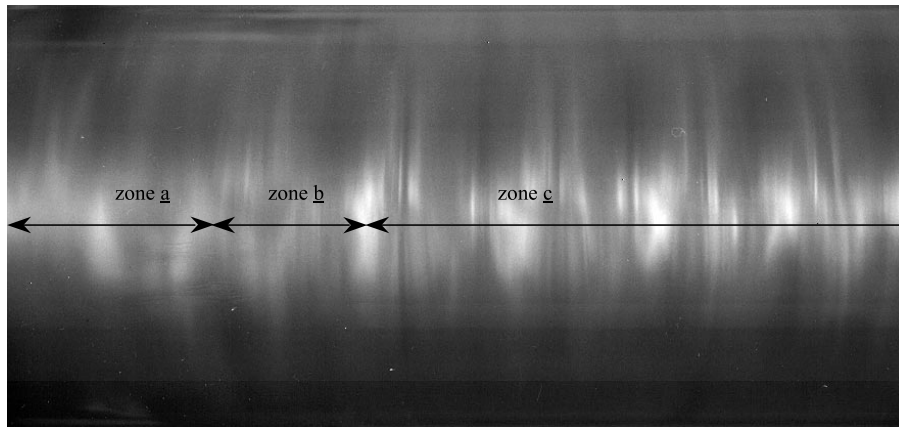


Fig. 9. View of vortex flow at the inlet of the SSHE for a Newtonian solution (2 blades; $Ta_g = 110$; $N = 5.9$ rps; $Q = 35 \text{ l h}^{-1}$; $Re_{axg} = 1.9$). Zone *a* – without vortices; zone *b* – birth-place of vortices and zone *c* – developed vortices.

- *zone c*: vortices acquire stability and move throughout the exchanger towards to the outlet where zone *b* then zone *a* reappear.

Consequently, visualisations show that the geometry of bowls and blades deeply influences the flow pattern at the edges of the equipment. Exploitation of the limiting diffusion current given by the probes allows completing these results.

Fig. 10(a) shows an example of the general evolution of I with respect to time for a non-Newtonian CMC solution. The evolution of I is the same for every value of Ta_g and for the different fluids used (Newtonian solutions, non-Newtonian solutions of CMC and guar). This representation indicates that the limiting diffusion current is fully controlled by the rotation of blades (for each value of Ta_g). Fig. 10(b) shows that minimum values of the diffusion current in presence of blades are significantly greater than those in an annulus without blades (laminar and vortex flows). The vortex flow pattern is renewed at each blade passage, thereby resulting in an unsteady vortex flow which by nature is different from Taylor vortices. Actually, the scraping of the microelectrodes is very fast and creates large fluctuations. Fig. 10(b) shows the predominance of scraping effects under vortices effects. Sometimes, in particular situations of buckling up of the blades, the clearance between the edge of the blade and the wall may become so thin that no electrolyte occurs on the

microelectrode. In this case, a signal interruption is recorded.

3.1.3. Discussion

Comparison of Figs. 6 and 9 shows that noticeably different flow patterns in SSHE occur from those observed in an annular space in the same conditions. The formation of vortices is thwarted by the blades (and by the clips of the blades) and upstream motion (from zone *b* to zone *a*, Fig. 5) of the vortices formation in the direction of the inlet bowl is observed. Furthermore, visual observations show that the transition between laminar and vortex flows in SSHE occurs for a different critical value of Taylor number ($Ta_{gc} \approx 80$) than the one determined in an annulus ($Ta_{gc} \approx 45$). These results differ from the main conclusion of the literature which assumes that flow patterns in SSHE and in annulus are fundamentally comparable (Härröd, 1986; Abichandani et al., 1987). Yet, flow patterns visualisations in SSHE are scarce. Trommelen and Beek (1971a) carried out a study of the flow pattern in SSHE with a glass outer wall. These authors, who visualised Taylor vortices by dispersing small polyethylene beads in glycerol/water solutions, declared that the transition from Couette flow to Taylor vortices could not be observed very accurately. Unfortunately, Trommelen and Beek (1971a) did not provide photographs of Taylor vortices and restricted their study to the Couette flow regime.

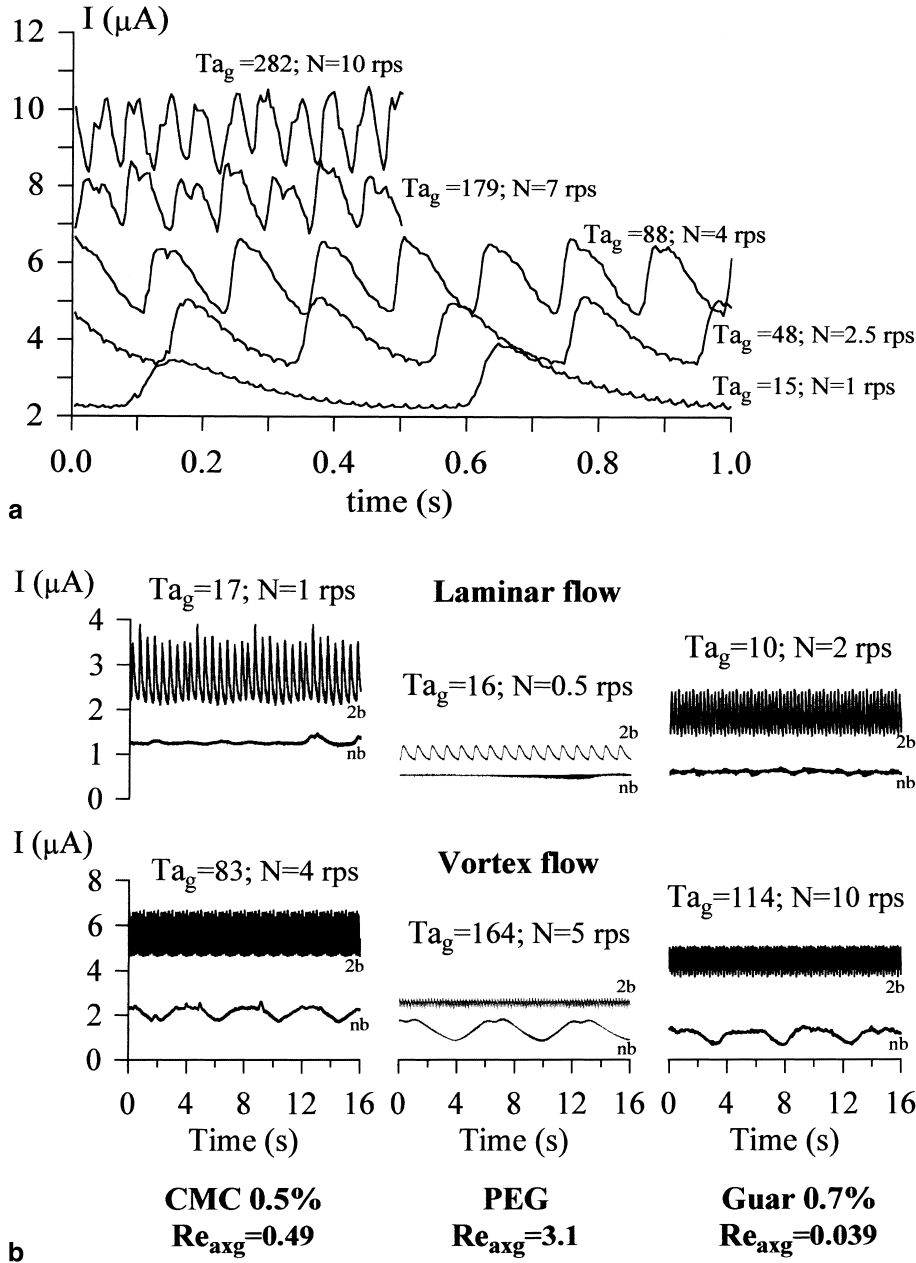


Fig. 10. (a) Time evolution of limiting diffusion current for a non-Newtonian solution of 0.5% CMC in SSHE (2 blades; $Re_{axg} = 0.5$; $Q = 35 \text{ l h}^{-1}$); (b) comparison of recorded limiting diffusion current with respect to time in an annulus for three different solutions with and without blades ($Q = 35 \text{ l h}^{-1}$); nb – no blades; 2b – 2 blades.

Nevertheless, in their conclusion, these authors strangely established that the flow is either in the Couette flow regime or in the Taylor vortices regime (with description of Taylor cells like those observed in an annulus) and that critical Reynolds number of rotation is equal to that for flow in the annulus. More recently, Burmester et al. (1996) carried out visualisation studies in a SSHE in which the shell was replaced by a Perspex tube. A non-Newtonian model fluid (0.4% w/w Carbopol EDT 2001) with similar rheological properties to those of food products is used. High-density polyethylene particles (sieved below $100 \mu\text{m}$) are added to this

fluid. It is observed that particles streak followed parallel streamlines indicating that the rotational flow is in the laminar regime. No evidence of Taylor vortices can be seen in the photographs taken, as expected from the range of Ta_g studied ($Ta_g < 32$). Lastly, Burmester et al. (1996) established an increase in backmixing with increasing rotor speed in laminar flow.

Trommelen and Beek (1971a) and Burmester et al. (1996) visual results, associated with those of the present work, shows that no transition between laminar and vortex flow occurs at low values of Taylor number in SSHE (as suggested in Benezech (1988)). Consequently,

the phenomena of appearance and disappearance of temperature heterogeneities observed in the industrial SSHE for $Ta_g \approx 10$ (Dumont et al., 2000a) cannot be attributed to the change in the flow pattern within the exchanger. The observed hydrodynamic perturbations and backmixing located at the edge of the apparatus, and generated by the geometry of bowls and shaft and by flowrate, could lead to a change of thermal behaviour inside the bowls and could explain the thermal heterogeneities within the exchanger. It is interesting to note that the disturbances observed at the edges of the SSHE differ from the numerical analyses of Baccar and Abid (1997) which showed that a pair of rotating vortices occurred in the edges of the apparatus. Nevertheless, numerical method used by these authors did not integrate the entrance effects into the imposed boundary conditions.

3.2. Wall shear rates

3.2.1. Without blades

For the laminar flow, S is independent of the axial position of the microelectrode ($I = \text{cte}$ and $\bar{S} = S$) and linearly increases with N according to Eq. (2) obtained from the Couette flow velocity profile for a power-law fluid ($n = 1$, for Newtonian solutions)

$$\frac{\bar{S}}{N} = \frac{4\pi}{n} \frac{R_r^{2/n}}{(R_s^{2/n} - R_r^{2/n})}. \quad (2)$$

Eq. (2) shows that \bar{S}/N ratio is independent of Ta_g in laminar regime. At $Ta_g > Ta_{gc}$, when Taylor vortices are developed, the electrochemical method allows to obtain axial measurements of wall shear rate continuously on the body of the Taylor cells. Visual observations show that the outflow boundary (M) and the inflow boundary (m) bound the Taylor cells. S_M and S_m correspond to the

value of the mean wall shear for, respectively, each boundary (Fig. 5). The value of S is higher for outflow than for inflow. The value given by any probe is located between S_M and S_m and the average wall shear rate \bar{S} is given by $\bar{S} \cong (S_M + S_m)/2$. For a given microelectrode, an example of the dimensionless representation of the mean wall shear rate is presented in Fig. 11. This representation allows one to verify the theoretical value of the \bar{S}/N ratio in laminar regime (Eq. (2)) and to detect the transition between laminar and vortex flows, i.e., when \bar{S}/N ratio becomes a Ta_g function. Fig. 11 shows that experimental measurements of \bar{S}/N ratio in the laminar flow agree with theoretical value given by Eq. (2) for very viscous Newtonian solutions. The same agreement is obtained for non-Newtonian CMC solutions (Fig. 13). But in the case of non-Newtonian guar solutions, results obtained show that \bar{S}/N decreases with Ta_g in the laminar regime though that \bar{S}/N ratio order of magnitude agrees with Eq. (2). Viscoelastic effects should be considered. Fig. 11 also shows that vortices appearance moderately increases the mean wall shear rates which attains 200 s^{-1} for the maximal rotational speed ($\bar{S}/N \approx 20$ when $N = 10 \text{ rps}$).

3.2.2. With 2 blades

In the general case of scraping without signal interruption, the very fast large fluctuations of the limiting diffusion current do not allow one to calculate the wall shear rates using Eq. (1). Indeed, instantaneous wall shear rate can be related to the instantaneous limiting current only in the case of quasi-steady flows (Dumont, Fayolle & Legrand, 2000b). The main difficulty in interpreting electrodiffusion measurements comes from the need to consider the dynamic response of the concentration boundary layer at the probe surface to flow fluctuations. Sobolík, Wein and Cermak (1987) propose

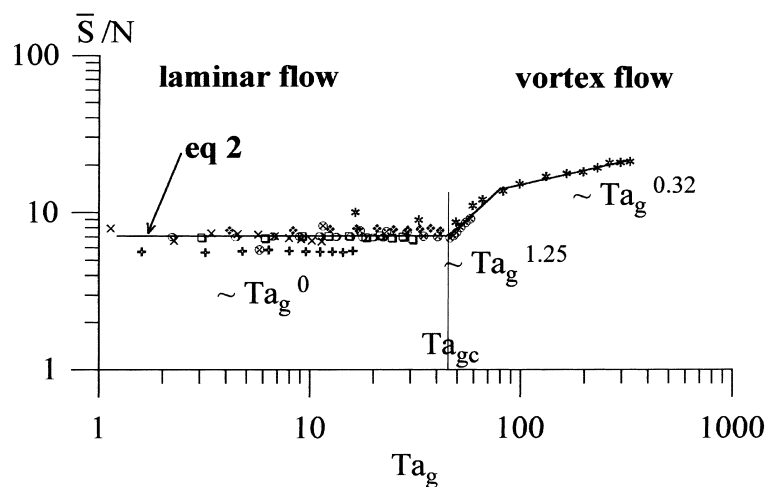


Fig. 11. Dimensionless representation of wall shear rates with respect to Ta_g in an annulus without blades for Newtonian solutions ($Q = 35 \text{ l h}^{-1}$). (X) – HV45-80; (+) – HV45-75; (O) – HV45-70; (□) – HV45-65; (◆) – HV45-60; (⊗) – HV45-55; (*) – PEG.

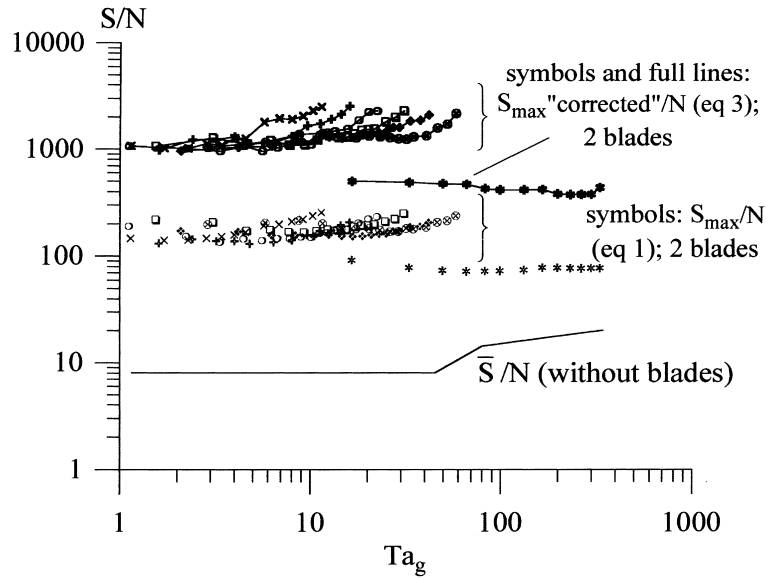


Fig. 12. Evolution of S_{max}/N (calculated both with Eqs. (1) and (3)) with respect to Ta_g for Newtonian solutions in SSHE (2 blades). Comparison with (\bar{S}/N) measured in an annulus without blades. (X) – HV45-80; (♦) – HV45-75; (O) – HV45-70; (□) – HV45-65; (◆) – HV45-60; (⊗) – HV45-55; (*) – PEG.

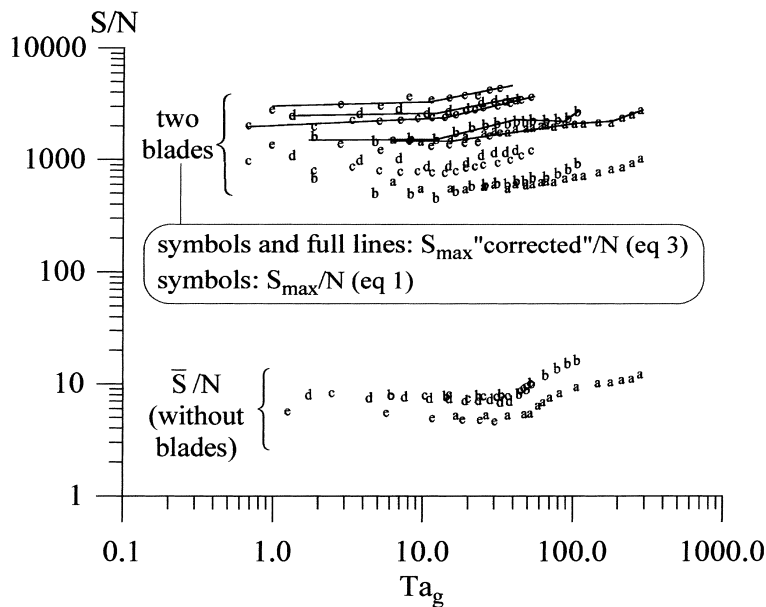


Fig. 13. Evolution of S_{max}/N (calculated both with Eqs. (1) and (3)) with respect to Ta_g for non-Newtonian CMC solutions in SSHE (2 blades). Comparison with (\bar{S}/N) measured in an annulus without blades. (a) 0.5% CMC; (b) 0.7% CMC; (c) 0.9% CMC; (d) 1.0% CMC; (e) 1.1% CMC.

a model that enables calculation of instantaneous wall shear rate from the measuring limiting diffusion current even at large flow fluctuations (Eq. (3))

$$S_c(t) = S(t) + \frac{2}{3}t_0 \left(\frac{\partial S}{\partial t} \right), \tag{3}$$

where $S_c(t)$ is the value of the wall shear rate corrected with respect to “microelectrode inertia”, $S(t)$ the quasi-steady interpretation of the measured current (Eq. (1)),

and t_0 is the characteristic time of the microelectrode. S and S_c have been calculated in scraping situations in order to obtain the maximal value of wall shear rate (S_{max}) and to deduce the clearance between the edge of the blade and the wall of the stator. However, the current variations are so fast (high values of dI/dt) that corrections are difficult to calculate accurately. Thus, the actual value of S_{max} should be included between the wall shear rate S calculated using Eq. (1) and the “corrected”

wall shear rate S_c calculated using Eq. (3). These wall shear rate curves are both compared in Figs. 12 and 13. For comparison, these figures also show the evolution of the ratio (\bar{S}/N) obtained without blades. We had also calculated the minimal value of wall shear rate S_{\min} corresponding to the wall shear rate between two scrapings. Figs. 14 and 15 show the evolution of S_{\min}/N with respect to Ta_g for Newtonian and non-Newtonian CMC solutions. Figs. 12–15 clearly reveal that wall shear rates in SSHE are noticeably different from those observed in an annulus without blades. Two observations can be mentioned. First, wall shear rates in SSHE (S_{\max} and S_{\min}) are 10–100 higher than those measured in an annulus under the same conditions. Second, it is

not possible to determine the transition between laminar and vortex flow which agrees with visual observations as in an annulus without blades. It is not in contradiction with the good running of the electrochemical technique. In the annulus without blades, probes detect vortices appearance because it leads to a great change of wall shear rates. In that case, wall shear rates analyses agree with visual observations. In the case of SSHE with two blades, Fig. 10(a) and (b) clearly show that vortices appearance represents a minor phenomenon for the wall shear rates point of view; the major phenomenon being represented by the blades scrapings. Thus, wall shear rates analyses (Figs. 12–15) reveal this fact. Vortices appearance cannot be detected because its influence

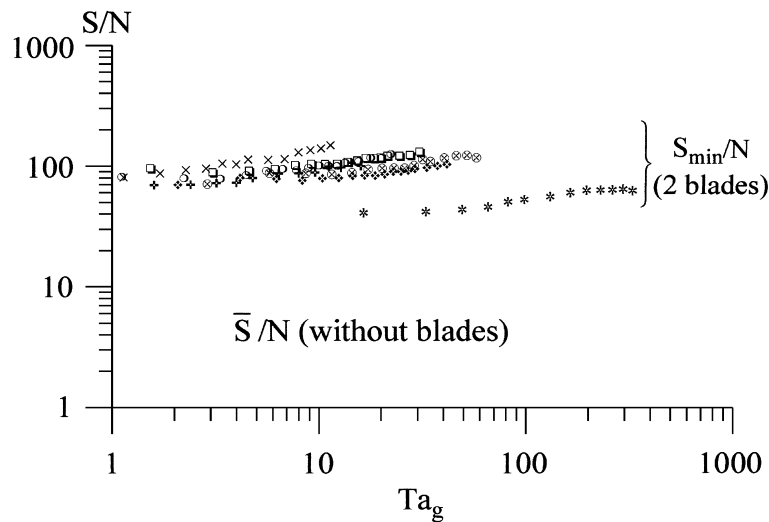


Fig. 14. Evolution of S_{\min}/N with respect to Ta_g for Newtonian solutions in SSHE (2 blades). Comparison with (\bar{S}/N) measured in an annulus without blades. (X) – HV45-80; (+) – HV45-75; (O) – HV45-70; (□) – HV45-65; (◆) – HV45-60; (⊗) – HV45-55; (*) – PEG.

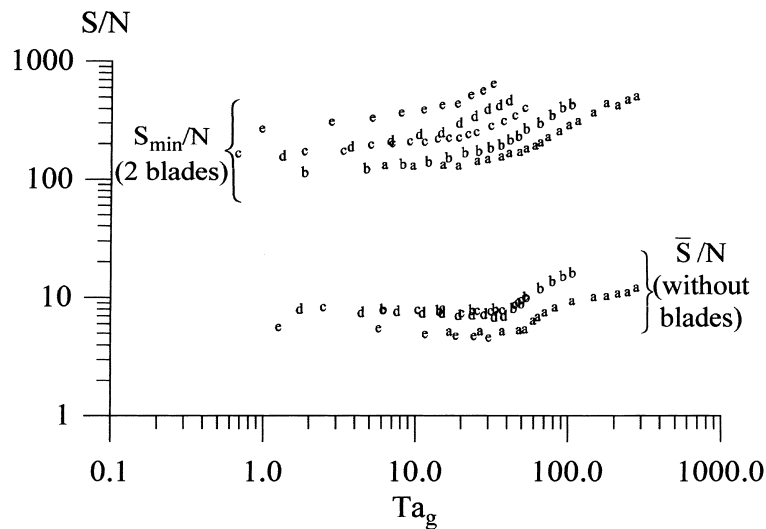


Fig. 15. Evolution of S_{\min}/N with respect to Ta_g for non-Newtonian CMC solutions in SSHE (2 blades). Comparison with (\bar{S}/N) measured in an annulus without blades. (a) 0.5% CMC; (b) 0.7% CMC; (c) 0.9% CMC; (d) 1.0% CMC; (e) 1.1% CMC.

appears negligible in comparison with the one of scraping. The changes of evolution of \bar{S}/N ratio (S_{\max}/N and S_{\min}/N), which appear for low and different values of Ta_g , seem to be linked to rheological properties of solutions. It is possible that phenomenon like viscous heating of the liquid between the edge of the scraper blade and the wall, which should be considerable (Trommelen & Beek, 1971b), can explain these shifts. Specific properties of solutions (slip effect) also may be considered.

3.2.3. Discussion

Some models of the shear rates in SSHE are proposed in the literature (Table 4) and are compared with our experimental data (Figs. 12–15). The model of Trommelen and Beek (1971b) is specifically devoted to the transition of the local shear rate corresponding to a scraping of the tube wall. Trommelen and Beek (1971b), who developed a formula to estimate the power requirements for the blades in a SSHE, supposed that the edge of the blade is rectangular and the velocity profile between scraper blade and tube wall is linear. From a series of measurements of power consumption and from the theoretical considerations of Penney and Bell (1967), Trommelen and Beek (1971b) concluded that the clearance between the edge of the scraper blade and tube wall (δ) is of the order of 1×10^{-6} m. In this case, the local shear rate $\dot{\gamma}$ (Eq. (4), Table 4) can be estimated as several hundreds of thousands per second. In our case, experimental determination of S_{\max} (Figs. 12 and 13) allowed calculation of δ using Eq. (4). The lowest value of δ determined in this way is 50×10^{-6} m. This experimentally measured value is more important than the one calculated by Trommelen and Beek (1971b). Yet, it could be found that, in the case of deformation of the blades (buckling), δ can be locally less than this value. More recently, Toh and Murakami (1982) analytically calculated the power requirements for floating blades.

They consider the shape of the blades, the number of blades, the scraping angle of the blades and the slit of the blades. But the equations obtained by the mechanical approach, which are very voluminous and complex, do not allow calculation of the clearance between the edge of the scraper and the stator. The other models (Leuliet, Maingonnat & Corrieu, 1986; Maingonnat, Leuliet & Benezech, 1987; Naimi, 1989; Härröd, 1990a) are more generally devoted to an estimation of a global wall shear rate in the exchanger. Thus, the models of Leuliet et al. (1986) and Maingonnat et al. (1987), based on investigations of pressure drop, propose the calculation of the average shear rate in SSHE (Eqs. (5) and (6), Table 4). Using industrial conditions, these models show that $\dot{\gamma}$ is equivalent to the shear rates calculated in a Couette system without blades. In the same way, the model of Naimi (1989) suggests that the average shear rate in SSHE (Eq. (7), Table 4) is equivalent to the shear rate in an annulus because the term U_d is negligible with respect to the term $(2\pi R_r N)$ and the effects of the blades are not considered. Lastly, the method proposed by Härröd (1990a) seems to be the most simple of all (Eq. (8), Table 4) because the average wall shear rate proposed by this author is estimated as the arithmetic mean of the shear rate at the tube wall and at the shaft for Newtonian fluids. From Härröd (1990a), the method can be expected to be good for a SSHE if the affects of axial flow, blades and others design factors can be neglected. The average shear rates corresponding to these different models (Eqs. (5)–(8), Table 4) do not exceed $\approx 100 \text{ s}^{-1}$ or $\approx 200 \text{ s}^{-1}$. Yet, our local measurements, which complete the different global models, show that shear rates can be very high in scraping situations. These measurements represent a very interesting information especially for the mechanical fragile food products. Nevertheless, wall shear rate measurements at the shaft must be realised in order to complete these first results and to confirm the validity of the different global models.

Table 4
Models of shear rates proposed in the literature

Authors	Models	Remarks
Trommelen and Beek (1971b)	$\dot{\gamma} = \frac{2\pi R_s N}{\delta}$	(4) Estimation of δ : 10^{-6} m
Leuliet et al. (1986)	$\dot{\gamma} = (3.213 \times 10^4 + 1.45^n n^{-0.7115} Q + 23.44 Q^{-0.03} n^{0.1754} N)$	(5) Laminar flow
Maingonnat et al. (1987)	$\dot{\gamma} = \xi 1.3^n Q + \beta N$	(6) β and ξ are given by charts
Naimi (1989)	$\dot{\gamma} = \frac{2\sqrt{U_d^2 + (2\pi R_r N)^2}}{d_h}$	(7) –
Härröd (1990a)	$\dot{\gamma} = \frac{d_s^2 + d_r^2}{d_s^2 - d_r^2} (2\pi N)$	(8) Only if the effects of axial flow, blades and others design factors can be neglected

4. Conclusion

Our investigations in a scaled-down model of an industrial exchanger, visual observations and wall shear rates measurements, show that hydrodynamics in a SSHE and in an annulus are not comparable:

1. The transition between laminar and vortex flows in SSHE occurs for a critical value of generalised Taylor number ($Ta_g \approx 80$) greater than the one determined in an annulus ($Ta_g \approx 45$) for the same conditions. Furthermore, the formation of vortices is thwarted by the blades and falling motion of the vortices in formation in direction of the inlet bowl are observed. The disturbances of the flow patterns at the edges of the exchangers, created by the geometry of bowls and shaft, could explain, instead of flow regime change, the dramatic change of thermal behaviour observed in industrial SSHE.
2. In contrast to wall shear rates in an annulus, which depend on the flow regime, the wall shear rates in a SSHE appears fully controlled by the rotation of the blades. For the wall shear rates point of view, the vortices have a negligible influence in comparison with the one of blade scrapings. Then, wall shear rates due to blade scrapings can reach up to $40\,000\text{ s}^{-1}$. Under these conditions, the lowest value of the clearance between the edge of the blades and the stator is about $50 \times 10^{-6}\text{ m}$.

References

- Abichandani, H., Sarma, S. C., & Heldman, D. R. (1987). Hydrodynamics and heat transfer in liquid full scraped surface heat exchangers. A review. *Journal of Food Process Engineering*, 9, 121–141.
- Baccar, M., & Abid, M. S. (1997). Numerical analysis of three-dimensional thermal behaviour in a scraped-surface heated exchanger. *Récents Progrès en Génie des Procédés*, 11 (51), 219–226.
- Benezech, T. (1988). *Etude de la distribution des temps de séjour, des performances thermiques et de la consommation de puissance d'échangeurs de chaleur à surface raclée traitant des produits non-Newtoniens*. Ph.D. thesis. INP Lorraine.
- Burmester, S. S. H., Winch, P. J., & Russell, A. B. (1996). A flow visualisation technique to characterise the mixing in a scraped surface heat exchanger. *International Chemical Engineering Research Event*, 2, 865–867.
- DiPrima, R. C. (1960). The stability of a viscous fluid between rotating cylinders with an axial flow. *Journal of Fluid Mechanics*, 9, 621–630.
- Dumont, E., Della Valle, D., Fayolle, F., & Legrand, J. (2000a). Influence of flow regimes on temperature heterogeneities within a scraped surface heat exchanger. *Journal of Food Process Engineering* (in press).
- Dumont, E., Fayolle, F., & Legrand, J. (1999). Determination of hydrodynamic properties in an industrial scraped surface heat exchanger and its scale-down model. *Récents Progrès en Génie des Procédés*, 13 (71), 401–409 (Ed. Tec-Doc, Lavoisier).
- Dumont, E., Fayolle, F., & Legrand, J. (2000b). Electrodiffusional wall shear rate analysis in scraped surface heat exchanger. *AIChE Journal* (accepted).
- Esser, A., & Grossmann, S. (1996). Analytic expression for Taylor–Couette stability boundary. *Physic Fluids*, 8, 1814–1819.
- Giordano, R. C., Giordano, R. L. C., Prazeres, D. M. F., & Cooney, C. L. (1998). Analysis of a Taylor–Poiseuille vortex flow reactor. I. Flow patterns and mass transfer characteristics. *Chemical Engineering Science*, 20, 3635–3652.
- Härröd, M. (1986). A literature survey of flow patterns, mixing, residence time distribution heat transfer and power requirements. *Journal of Food Process Engineering*, 9, 1–62.
- Härröd, M. (1990a). Methods to distinguish between laminar and vortical flow in scraped surface heat exchanger. *Journal of Food Process Engineering*, 13, 39–57.
- Härröd, M. (1990b). Modelling of vortical heat transfer in scraped surface heat exchanger. *Journal of Food Process Engineering*, 13, 79–111.
- Härröd, M. (1990c). Temperature variations in the outlet from scraped surface heat exchanger. *Journal of Food Process Engineering*, 13, 23–28.
- Legrand, J., Dumont, E., Comiti, J., & Fayolle, F. (2000). Diffusion coefficients of ferricyanide ions in polymeric solutions – comparison of different experimental methods. *Electrochimica Acta* 45, 1791–1803.
- Leuliet, J. C., Maingonnat, J. F., & Corrieu, G. (1986). Etude de la perte de charge dans un échangeur de chaleur à surface raclée traitant des produits Newtoniens et non-Newtoniens. *Journal of Food Engineering*, 5, 153–176.
- Maingonnat, J. F., Leuliet, J. C., & Benezech, T. (1987). Modélisation de la vitesse de cisaillement apparente dans un échangeur de chaleur à surface raclée. Application aux performances thermiques avec des produits non-Newtoniens. *Revue Générale de Thermique*, 306–307, 381–385.
- Miyauchi, T., & Vermulen, T. (1963). Longitudinal dispersion in two phase continuous flow operations. *Industrial and Engineering Chemistry Fundamentals*, 2 (2), 113–126.
- Naimi, M. (1989). *Etude des lois d'écoulement et de transfert de chaleur pour des fluides non-Newtoniens en espace annulaire tournant. Approche réaliste de l'échangeur de chaleur à surface raclée*. Ph.D. thesis, ENSEM-LEMTA, INP Lorraine.
- Penney, W. R., & Bell, K. J. (1967). Close-clearance agitators. Part 1. Power requirements. *Industrial and Engineering Chemistry*, 59 (4), 40–46.
- Reiss, L. P., & Hanratty, T. J. (1963). An experimental study of the unsteady nature of the viscous sublayer. *AIChE Journal*, 8 (2), 154–160.
- Sobolík, V., Wein, O., & Cermak, J. (1987). Simultaneous measurement of film thickness and wall shear stress in wavy flow of non-Newtonian liquids. *Collection Czechoslovak Chemical Communications*, 52, 913–928.
- Toh, M., & Murakami, Y. (1982). Power consumption of a fluid-floating scraper blade. *Journal of Chemical Engineering of Japan*, 15 (6), 493–495.
- Trommelen, A. M., & Beek, W. J. (1971a). Flow phenomena in a scraped surface heat exchanger. *Chemical Engineering Science*, 26, 1933–1942.
- Trommelen, A. M., & Beek, W. J. (1971b). A mechanism for heat transfer in a votator-type scraped-surface heat exchanger. *Chemical Engineering Science*, 26, 1977–1986.
- Wronski, S., & Jastrzebski, M. (1990). Experimental investigations of the stability limit of the helical flow of pseudoplastic liquids. *Rheologica Acta*, 29, 453–461.